International Journal of Civil Engineering and Technology (IJCIET)
Volume 9, Issue 5, May 2018, pp. 1380–1391, Article ID: IJCIET_09_05_151
Available online at http://www.iaeme.com/ijciet/issues.asp?JType=IJCIET&VType=9&IType=5
ISSN Print: 0976-6308 and ISSN Online: 0976-6316

SEISMIC PERFORMANCE OF BASE-ISOLATED STIFFENED CORRUGATED STEEL SILOS WITH LEAD RUBBER BEARINGS

Zaoui D, Djermane M
Department of Civil Engineering,
FIMAS Laboratory Tahri Mohmed University, Bechar Algeria

ABSTRACT

The paper deals with the behavior of cylindrical metal silos composed of horizontally corrugated sheets strengthened by vertical open-sectional thin-walled columns. The aim of three-dimensional finite element analysis taking into account the complexity of the whole structure (corrugated form, open-sectional thin-walled stiffeners, conical form for the roof and the hopper) and the use of lead-plug bearings device for the base isolation was to evaluate the feasibility of the bearings isolator to ensure an adequate performance of the studied silo structure namely to avoid the buckling risk of the vertical open-sectional stiffeners. The response frequency and the time-history analyses under the 1970 San Fernando ground motion results show average reductions of the global base shear and overturning moment, the energy dissipation provided by the lead rubber bearings isolator has assured the bearing capacity recommended by the Eurocode rules and avoid the buckling failures observed in the thin-walled stiffeners.

Keywords: Buckling Bearing Capacity, Eurocode Guidelines, Finite Element Analysis, Lead Rubber Bearings, Seismic Isolation, Stiffened Corrugated Steel Silos.

Cite this Article: Zaoui D and Djermane M, Seismic Performance of Base-Isolated Stiffened Corrugated Steel Silos with Lead Rubber Bearings, International Journal of Civil Engineering and Technology, 9(5), 2018, pp. 1380–1391.
http://www.iaeme.com/ijciet/issues.asp?JType=IJCIET&VType=9&IType=5

1. INTRODUCTION

Metal silos are frequently built of thin-walled horizontally corrugated curved sheets strengthened by vertical stiffeners (columns) distributed uniformly around the silo circumference and connected with screws due to an economical steel consumption and a small silo weight [1] [2]. In those silos, horizontally corrugated wall sheets carry horizontal tensile forces caused by horizontal wall pressure of a bulk solid and vertical columns carry vertical compressive forces exerted by wall friction stress from a bulk solid [3] [4]. Under loading; the vertical compression failure of the corrugations under vertical loading may not cause

catastrophic collapse, but may cause lean of the structure and out-of-roundness, effectively requiring major repair. It can also lead to buckling failure with potentially catastrophic results [5] [6]. (See Fig. 1)

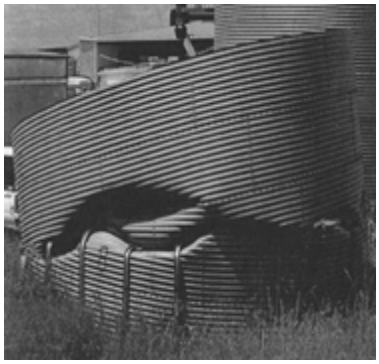

Corrugation failure at stiffener end [5]

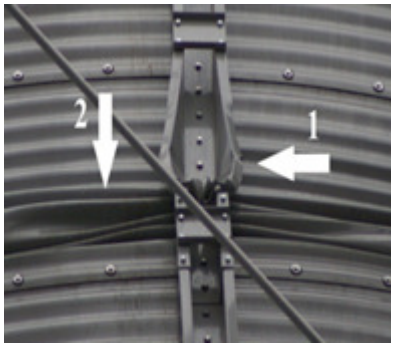

1 – damage to stringer; 2 – damage to sheathing [6]

Figure 1 Buckling failures of stiffened corrugated steel silos

To the author's knowledge, there have been few studies deal to the dynamic stability of cylindrical metal bin: Uckan et al. [7], Castiglioni and Kanyilmaz [8], Gigliotti et al. [9], Morelli et al. [10], Pinkawa et al. [11], Kanyilmaz and Castiglioni [12], Salvatore et al. [13]. Therefore, it will be interesting to investigate the stability of this kind of storage structures particularly those composed of horizontally corrugated sheets strengthened by vertical open-sectional thin-walled columns widely used in practices. On the other hand, to examine the feasibility of their base isolation, such technique become quite popular and efficient in the mitigation of seismic effects on building and bridge constructions [14].

The response frequency and the time-history analyses under the 1970 San Fernando ground motion results obtained in this paper show average reductions of the global base shear and overturning moment, the energy dissipation provided by the lead rubber bearings isolator has assured the bearing capacity recommended by the Eurocode rules and avoid the buckling failures observed in the thin-walled stiffeners.

2. EUROCODE GUIDELINES FOR STIFFENED CORRUGATED STEEL SILO DESIGN

Described in [15]; three types of buckling forms may be observed according to EC3 [16] in stiffened corrugated steel silo: local, distortional and global buckling. Local instabilities occur when some wall parts of profile cross-sections have characteristic single bulges (Fig. 2(a)). The distortional instability is characterized by deformation of profile side walls which alternately bend to the inside and outside (Fig. 2(b)). Finally; the global column buckling shape, which is closer to the classical Euler one (Fig. 2(c)).

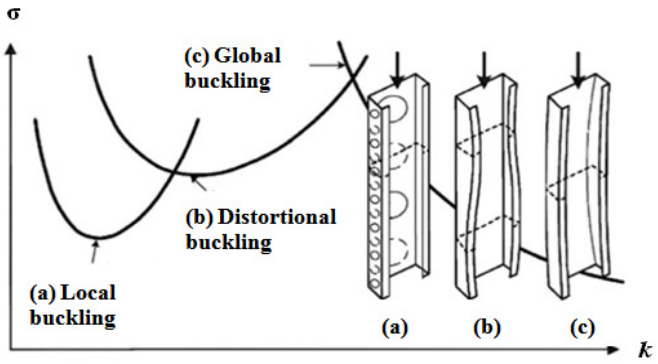

Figure 2 Single column buckling stress σ versus half-wave length *k* and buckling form under vertical load: (a) local buckling, (b) distortional buckling and (c) global buckling [15]

The critical buckling resistance $N_{b,RD}$ according the Eurocode 1 rules [16] should be calculated assuming uniform compression on the cross-section (Fig. 3) at any level, as:

$$N_{b,RD} = \min\left(2\frac{\sqrt{E\, I_y\, K}}{\gamma_{M1}}, \frac{A_{eff}\, f_y}{\gamma_{M1}} \right) \quad (1)$$

where:

$E\, I_y$ is the flexural rigidity of the stiffener for bending out of the plane of the wall, A_{eff} is the effective cross-sectional area of the stiffener and $\gamma = 1.10$ is the partial factor for resistance of shell wall to stability;

K is the flexural stiffness of the sheeting determined assuming that the sheeting spans between adjacent vertical stiffeners on either side with simply supported boundary conditions, may be estimated as:

$$K = k_s \frac{D_y}{d_s^3} \quad (2)$$

where:

D_y Is the flexural rigidity of the sheeting for circumferential bending; be taken as:

$$D_y = 0.13\, E\, t\, d^2 \quad (3)$$

d_s is the separation of the vertical stiffeners, should not be more than $d_{s,max}$ given by

$$d_{s,max} = k_{dx} \left(\frac{r^2\, D_y}{C_y} \right)^{0.25} \quad (4)$$

were C_y is the equivalent membrane properties (stretching stiffness's) may be taken as:

$$C_y = E\, t \left(1 + \frac{\pi^2\, d^2}{4\, l^2} \right) \quad (5)$$

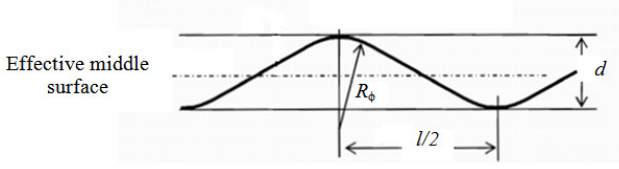

Figure 3 Corrugation profile and geometric parameters [16]

Where: d is the crest to crest dimension, t is the wavelength of the corrugation, R_ϕ is the local radius at the crest.

3. FINITE ELEMENT MODEL DESCRIPTION AND VALIDATION

The silo studied in this paper has a 21m high, 9.17m in diameter, the corrugation had 76mm pitch and 18mm depth. The silo was strengthened by 12 vertical columns composed of a varying cross-section and thickness along the column height. The silo roof and hopper were made from metal sheets inclined under an angle of 28 and stiffened by 28 radial beams. The silo structure rests on 12 tubular columns with X-braced members (Example shown in Fig. 4).

Figure 4 Example of stiffened corrugated steel with conical hopper [17]

Using ANSYS 14.5 [18] software library; the finite element simulation of the steel silo wall and stiffeners has been accomplished using an isoparametric shell element (SHELL281), which consists of an 8-noded element having six degrees of freedom at each node, for the silo support; the three-dimensional BEAM188 with 2-node and six degrees of freedom at each node is used. The base isolation device is simulated by the COMBIN 40 (combination of a spring-slider, damper and gap) element employed to reproduce the horizontal stiffness in two horizontal directions, to simulate the vertical stiffness; the COMBIN 14 (combination of a spring and damper) element is employed. (Figs. 5 (a) to (d) shows respectively the SHELL281, BEAM188, COMBIN 14 and the COMBIN 40 finite elements).

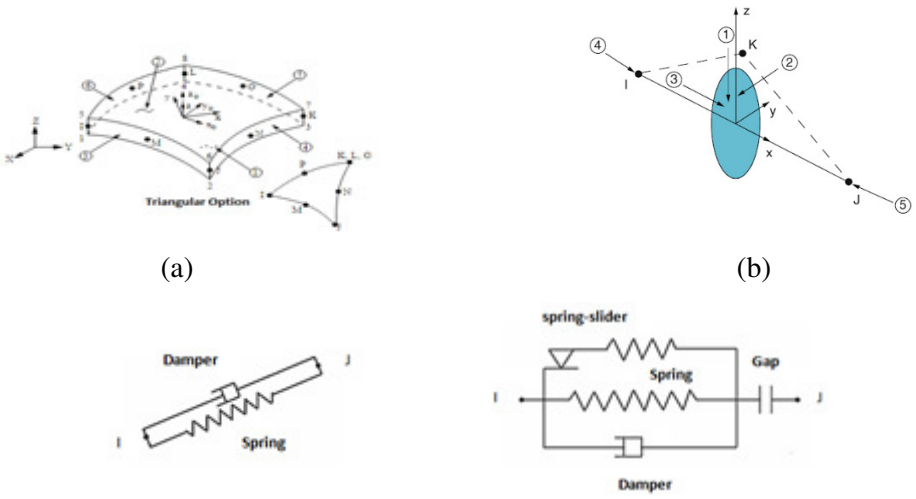

Figure 5 Finite elements used (a) for the silo wall, (b) for the support, (c) and (d) for the lead-plug bearing [15]

The behavior assigned to the wall material was of cinematic hardening, bilineal elastic-perfectly plastic, with a modulus of elasticity of 2.1e8kN/m^2, a Poisson's ratio of 0.3, a specific steel weight of 80kN/m^3 and an elasticity limit of 235MPa [19]. The bilinear model is adopted to provide the physical behaviour of the lead-plug bearings device. Fig. 6 shows an idealized bilinear model defined by the following parameters: *elastic stiffness*, k_e, *effective stiffness* k_{eff} , *post-yield stiffness*, k_p, and *characteristic strength*, Q:

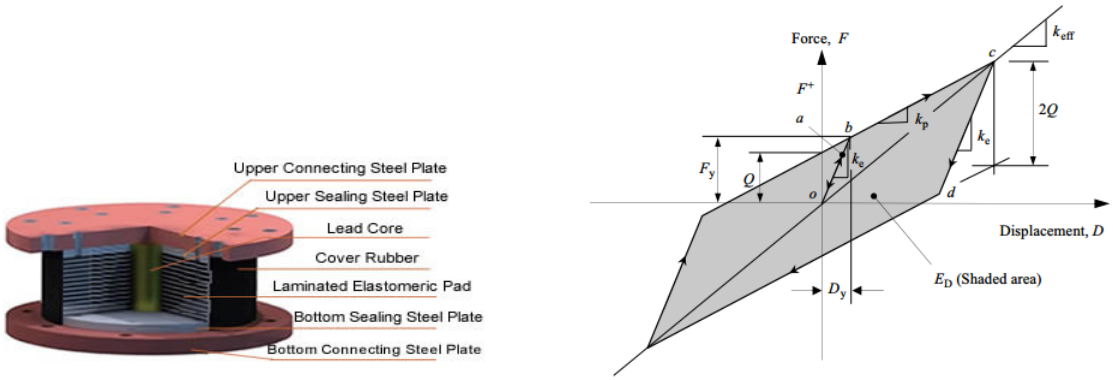

(a) (b)

Figure 6 Lead-plug bearings (a) Components and (b) Bilinear model [20], [21]

Effective stiffness of the bearing, at the post-yield region can be expressed in terms of the post-yield stiffness, k_p, and the characteristic strength, Q, with corresponding lateral displacement, D*; as:*

$$k_{eff} = k_p + \frac{Q}{D} \quad (6)$$

The yield displacement, D_y, is also derived from k_e, k_p, and Q:

$$D_y = \frac{Q}{k_e - k_p} \quad (7)$$

The yield force, F_y, at the yield displacement, D_y is determined as :

$$F_y = Q + k_p D_y \quad (8)$$

The characteristic strength, Q, of the lead-plug bearing is:

$$Q = A_l f_{yl} \quad (9)$$

The post-yield stiffness, k_p, is:

$$k_p = \frac{A_b G f_{yl}}{t} \quad (10)$$

where A_b is the bonded area of rubber; t is the total rubber thickness; lead yield stress, f_{yl},. the *tangent shear modulus* of rubber G.

The *effective damping* can be estimated in terms of Q, k_p, and κ the ratio of its elastic stiffness to post-yield stiffness as:

$$\beta_{eff} = \frac{2Q[((\kappa-1)k_p D - Q)]}{\pi(\kappa-1)k_p(k_p D + Q)\, D} \quad (11)$$

The specific value of the isolation period, T_d can be expressed as:

$$T_d = 2\pi \sqrt{\frac{W}{k_p\, g}} \quad (12)$$

Where W is the weight acting on an individual isolator and g is the gravitational acceleration constant.

According to Asif et al. [22]; there have been several studies investigating the optimum design values for the lead rubber bearings: Skinner et al. [23] suggested typical value of Q/W = 0.05 and k_e/k_p = 1/5 to 1/6 for moderate earthquakes, Park and Otsuka [24] compared different method to determine the yield ratio and recommended Q/W = 0.43 to 0.5 for moderate earthquakes, Naeim and Kelly [25] has given the design recommendations for k_e/k_p = 1/10, Jangid [26] recommended Q/W = 0.10 to 0.15 and T_d = 2.5 to 3s for near fault ground motions, Park et al. [27] the natural period of the isolated structure should be long enough to avoid the frequency range on which earthquake energy concentrates and short enough to resist the ambient vibration such as traffic or wind induced. Based on the previous investigations, the chosen values are Q/W = 0.10, T_d = 3s and k_e/k_p = 1/10.

Additional to the quasi-static effects due to filling state evaluated according to the Eurocode rules [28] ; the effect of the stored wheat matter due to the horizontal component of the seismic action on silo shell is introduced assuming that the particulate contents move together with the silo shell with a stiff behaviour without any amplification [29].

The earthquake motion selected for the study is the 1970 San Fernando earthquake, 164 Pacimoine record; the ground acceleration and the acceleration spectra for 2% of the critical damping are shown in Fig. 7. The peak ground acceleration (PGA) is 1.226g, the maximum ordinates of the pseudo-acceleration is 3.082g occurring at period 0.39s.

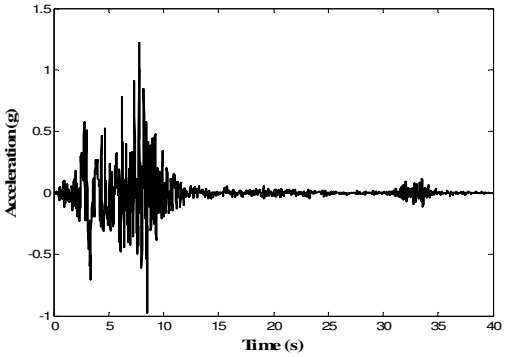

(a)

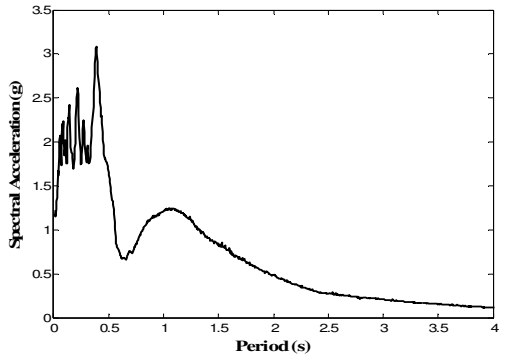

(b)

Figure 7 San Fernando 1970 earthquake (a) ground acceleration time histories and (b) spectral acceleration

The mesh density used in the established finite element model, is achieved by performing several nonlinear dynamic analyses with meshes more and more refined until having stable results and mesh independent. The Fig. 8 show the used mesh (the half for figure clarity) composed of 101376 shell elements, 492 beam elements and 12 isolator elements; which consist in totality 622086 degree of freedom.

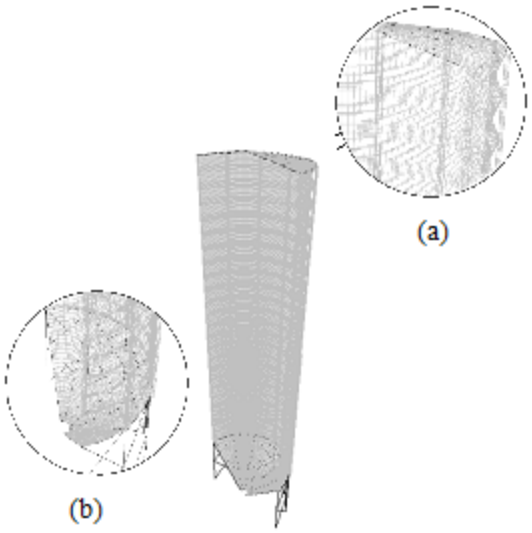

Figure 8 Established finite element model (a) zoom on Roof-Stiffener zone and (b) zoom on Hooper-Support zone

The validation of the established model for the base isolation device is carried out using a seismic response analysis of a liquid tank of Shekari et al. [30] (Equivalent mechanical model with two lumped masses; convective and impulsive) subjected to the 1970 San Fernando earthquake. Table 1 shows the material properties of the validation storage tank.

Table 1 Material properties of the validation storage tank (Shekari et al. [30]).

Tank dimensions and properties	
Radius	R = 7.32m
Height	h = 21.96m
Wall thickness	t = 0.0254m
Young's modulus	E_s = 206.7GPa
Poisson's ratio	μ_s = 0.3
Mass density	ρ_s = 7840kg/m^3 for steel and ρ_l=1000kg/m^3 for liquid
Isolation system properties	
Yield force	F_y = 240kN
Elastic stiffness	k_e = 28000kN/m
Post-elastic stiffness	k_p = 4200kN/m

The seismic responses of the validation tank were investigated for the two base conditions; fixed-base and isolated: for the first case we note a maximum of base shear force equal to 3.35MN and 1.125MN for the isolated base (respectively 4.8 % and 9.3 % of difference from Shekari et al. [29]), which allows to consider that validation of the model is achieved, it can be used for the next analysis.

5. RESULTS AND DISCUSSIONS

In this section, the effects of base-isolation on the response of the studied steel silo for the frequency analysis and for the transit analysis under the 1970 San Fernando earthquake ground motion are investigated.

a) Frequency analysis

The examination of the frequency contents of both systems fixed-base and isolated base; show that the effect of the isolation system is to soften the structure by the prolongation of the fundamental period to a larger value with regard to that non-isolated. The period is extended of 6 times; 0.479s for the restrained case and 3.09s for the isolated. Indeed, this period shift is the primary reason for the effectiveness of the isolation system, because its projection on the spectral acceleration curve of the considered earthquake produce 9 times of reduction (17.28g and 1.92g for the fixed-base the and isolated silo, respectively).

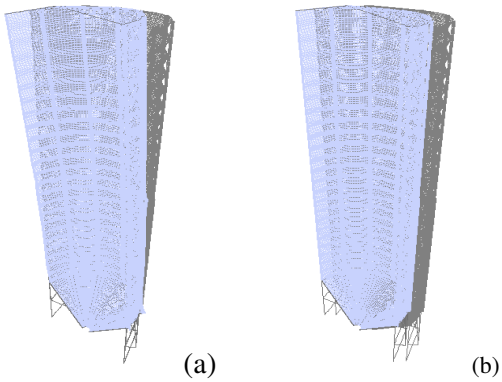

Figure 9 Modal deformed shape (a) Fixed-base and (b) Isolated-base

In terms of modal contribution; for the isolated silo; the fundamental mode has a modal contribution factor exceeding 90%; it means that the silo response is governed by the first mode with a pure translation, i.e. a rigid body movement, where the participation of higher modes becomes closer to zero. Unlike the restrained structure in which 30.13% and 27.18% are activated by the first and the second mode respectively with a restrained-beam vibration (See Fig. 9).

b) Time-history analysis

b-1) For silo base

The time variation of base shear force and overturning moment under the considered ground motion are illustrated in Figs. 10 (a) and (b). As a comparative the maximum base shear force for the fixed-base silo equal to 592.40kN at 8.42s is reduced to 67.03kN; or 88% of reduction, for the overturning moment the maximum equal to 3647kN.m at 8.61s corresponding to the non-isolated silo is decreased to 82.31kN.m; or 97% of decrease.

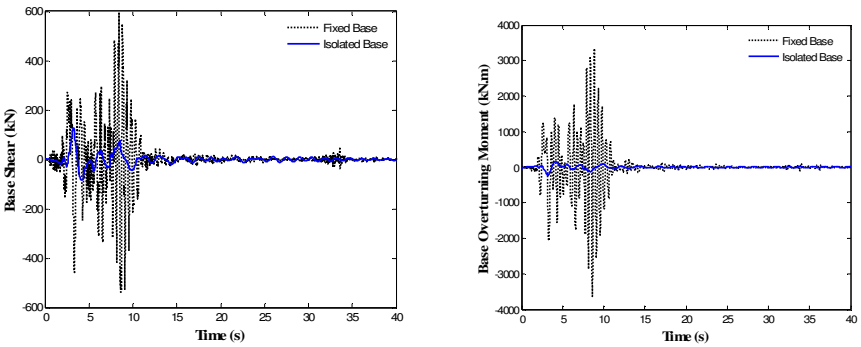

Figure 10 Time variation of (a) base shear force and (b) overturning moment under the 1970 San Fernando ground motion for the fixed-base and the isolated silo

On the Fig. 11 show the force-displacement curves of lead rubber bearing; the hysteresis loop producing an area of 1.778kN.m. This increase in energy dissipation of lead rubber bearing is due to the damping action produced by plastic deformation of the lead core enabling the post-yield stiffness.

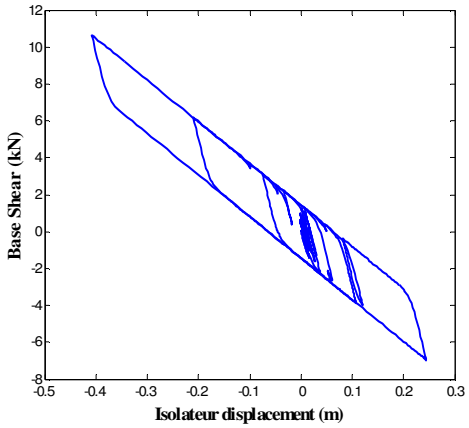

Figure 11 Hysteresis curve of lead rubber bearing under the 1970 San Fernando ground motion

b-2) For wall stiffeners

Figs. 12 and 13 present respectively the evolution of the efforts in the high and the bottom stiffener the more loaded (on the earthquake direction); it is clearly noticed that the establishment of the isolation device has limited the maximum effort to 37.23kN at 3.26s for the top stiffener (initially equal to 235kN at 8.27s) and to 102.20kN at 3.26s for the bottom stiffener (initially equal to 690.7kN at 8.29s).

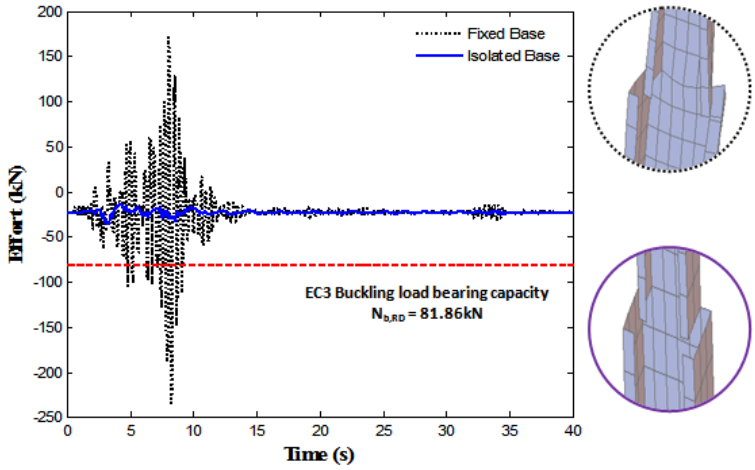

Figure 12 Stability of top stiffener under the 1970 San Fernando ground motion

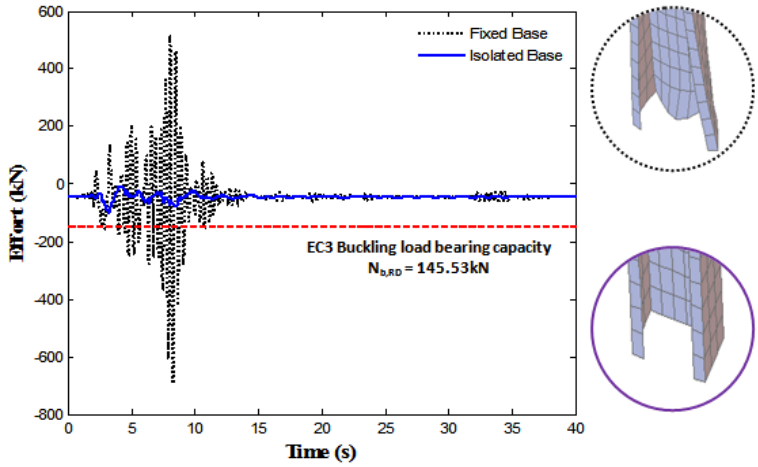

Figure 13 Stability of bottom stiffener under the 1970 San Fernando ground motion

In term of stability; the isolation device has ensured the bearing capacity of the stiffeners envisaged by the Eurocode rules (limited to 81.86kN for the top stiffener and 145.53kN for the bottom stiffener), clearly seen on the images captures relating to the buckled elements which correspond to the embedded silo and those not buckled of the isolated silo.

The above results indicate that due to base-isolation, whole system seismic response is reduced considerably, which ensure the stability of the studied steel silo.

6. CONCLUSION

The aim of three-dimensional finite element analysis established taking into account the complexity of the whole structure (corrugated form, open-sectional thin-walled stiffeners, conical form for the roof and the hopper) and the use of lead-plug bearings device for the base isolation; was to evaluate the feasibility of the bearings isolator to ensure an adequate performance of the studied silo structure namely to avoid the buckling risk of the vertical open-sectional stiffeners. The following conclusions can be drawn:

- The examination of the frequency contents of both systems fixed-base and isolated base; show that the effect of the isolation system is to soften the structure by the prolongation of the fundamental period to a larger value with regard to that non-isolated;
- The period projection on the spectral acceleration curve of the considered earthquake produce a reduction equal to 9 times (17.28g and 1.92g for the fixed-base and the isolated silo, respectively);
- In terms of modal contribution; the isolated silo response is governed by the first mode with a pure translation, i.e. a rigid body movement, where the participation of higher modes becomes closer to zero;
- Under the 1970 San Fernando ground motion; the maximum base shear force is reduced by 88% and 97% for the maximum overturning moment;
- The isolation device has ensured the bearing capacity of the stiffeners envisaged by the Eurocode rules, clearly seen on the images captures relating to the buckled elements which correspond to the embedded silo and those not buckled of the isolated silo.

ACKNOWLEDGEMENTS

This work was supported by FIMAS Laboratory, University of Tahri Mohammed Bechar, Algeria.

REFERENCES

[1] Wojcik, M., Iwicki, P. and Tejchman, J., 3D buckling analysis of a cylindrical metal bin composed of corrugated sheets strengthened by vertical stiffeners, Thin– Walled Structures, 49, 2011, 947–963.

[2] Iwicki, P. Rejowski, K. and Tejchman, J., Stability of cylindrical steel silos composed of corrugated sheets and columns based on FE analyses versus Eurocode 3 approach, Eng. Fail. Anal., 57, 2015, 444–469.

[3] Wójcik M., Iwicki P. and Tejchman J., 3D buckling analysis of a cylindrical metal bin composed of corrugated sheets strengthened by vertical stiffeners. Thin-Walled Structures 49, 8, 2011, 947-96

[4] Rejowski K., Iwicki P., Buckling analysis of cold formed silo column, Mech. Mech. Eng. 20 (2), 2016, 109–120.

[5] Ansourian, P., and Gläsle, M., Aspects of corrugated silos. Advances in Steel Structures (ICASS '02), 713–720.

[6] Ryszard Antonowicz, Czesław Bywalski and Mieczysław Kaminski, Analysis of loads and structural capacity of steel silo with corrugated wall for pelleted material, Journal of Civil Engineering and Management, 20:3, 2014, 372-379.

[7] Uckan E, Akbas B, Shen J, Wen R, Turandar K, Erdik M. Seismic performance of elevated steel silos during Van earthquake, October 23, 2011. Nat Hazards 2015;75:265–87.

[8] Castiglioni CA, Kanyilmaz A. Simplified numerical modeling of elevated silos for nonlinear dynamic analysis. Ing Sismica 2015;33(1–2):5–14.

[9] Gigliotti R, Faggella M, Rossi E, Ventrella M, Braga F. Performance based earthquake assessment of an industrial silos structure. ECCOMAS Congr 2016 VII Eur Congr Comput Methods Appl Sci Eng 2016:5–10.

[10] Morelli F, Piscini A, Salvatore W. Seismic retrofit of an industrial structure through an innovative self-centering hysteretic damper: Modelling, analysis and optimization. Proc. VII Eur. Congr. Comput. Methods Appl. Sci. Eng. M. Papadrakakis, V. Papadopoulos, G. Stefanou, V. Plevris (Editors), Crete Island, Greece, 2016, p. 5–10.

[11] Pinkawa M, Hoffmeister B, Feldmann M. Performance assessment of seismic retrofitting measures on silo structures using innovative seismic protection systems. ECCOMAS Congr. 2016 VII Eur. Congr. Comput. Methods Appl. Sci. Eng. M. Papadrakakis, V. Papadopoulos, G. Stefanou, V. Plevris, 2016, p. 5851– 67.

[12] Kanyilmaz, A., and Castiglioni, C. A., Reducing the seismic vulnerability of existing elevated silos by means of base isolation devices. Engineering Structures, 143, 2017, 477–497.

[13] Salvatore W, Morelli F, De Pasquale E, Tesi M, Degee H, Hofffmeister B, et al. EU-RFCS Project PROINDUSTRY (Seismic Protection of Industrial Plants by Enhanced Steel Based Systems; 2013). Final Report 2017.

[14] Matsagar V. A. and Jangid R. S., Base isolation for seismic retrofitting of structures, Pract. Period. Struct. Des. Constr. 13:4, 2008, 175–185.

[15] Hajko, P.; Tejchman, J.; Wojcik, M, Investigations of local/global buckling of cylindrical metal silos with corrugated sheets and open-sectional column profiles, Thin-Walled Structures Volume: 123 Pages: 341-350, 2018

[16] Eurocode 3, Design of steel structures, Part 1-6:Strength and Stability of Shell Structures, (European Committee for Standardization, 2007).

[17] Online agricultural exhibition, Retrieved March 15, 2018, from http://www.agriexpo.online/

[18] ANSYS Inc., ANSYS Version 14.5 User's Manual (Canonsburg, 2012).

[19] Juan A., Moran J.M., Guerra M.I., Couto A., Ayuga F. and Aguado P.J., Establishing stress state of cylindrical metal silos using finite element method: Comparison with ENV 1993, Thin Wall. Struct., 44, 2006, 1192-1200.

[20] Zaoqiang Dacheng Rubber Co., Ltd. Retrieved March 15, 2018, from http://www.bridgebearings.org

[21] Franklin Y. Cheng, Hongping Jiang, Kangyu Lou. Smart structures: innovative systems for seismic response control, (CRC Press, 2008)

[22] Asif Hameed, Min-Se Koo, Thang Dai Do, Jin-Hoon Jeong, Effect of lead rubber bearing characteristics on the response of seismic-isolated bridges, KSCE Journal of Civil Engineering, 2008, 12(3):187-196.

[23] Skinner, R. I., Robinson, W. H., and McVerry, G. H., An Introduction to Seismic Isolation, (Wiley, Chichester, England, 1993).

[24] Park, J. and Otsuka, H., Optimal yield level of bilinear seismic isolation devices, Earthquake Engineering and Structural Dynamics, Vol. 28, 1999, pp. 941-955.

[25] Naeim, F. and Kelly, J. M., Design of Seismic Isolated Structures: From Theory to Practice, (Wiley, Chichester, England 1999).

[26] Jangid, R.S., Optimum lead-rubber bearings for near-fault motions, Engineering Structures, Vol. 29, No. 10, 2006, pp. 2503-2513.

[27] Park, K.S., Jung, H.J., and Lee, I.W., A comparative study on aseismic performances of base isolation systems for multi-span continuous bridge." Engineering Structures, Vol. 24, No. 8, 2002, pp. 1001- 1013.

[28] Eurocode 1, Actions on structures, Part 4: Silos and tanks, (European Committee for Standardization, 2006).

[29] Eurocode 8, Design of structures for earthquake resistance, Part 1: General rules, seismic actions and rules for buildings, (European Committee for Standardization, 2004).

[30] Shekari, M. R., Khaji, N., and Ahmadi, M. T, On the seismic behavior of cylindrical base-isolated liquid storage tanks excited by long-period ground motions. Soil Dynamics and Earthquake Engineering, 30(10), 2010. 968–980.